inorganics

MDPI

Article

Efficient Disposal of Basic Fuchsin Dye from Aqueous Media Using $ZrO_2/MgMn_2O_4/Mg(Mg_{0.333}Mn_{1.333})O_4$ as a Novel and Facilely Synthesized Nanocomposite

Asma S. Al-Wasidi [1], Mohamed Khairy [2,3], Babiker Y. Abdulkhair [2,4] and Ehab A. Abdelrahman [2,3,*]

[1] Department of Chemistry, College of Science, Princess Nourah bint Abdulrahman University, P.O. Box 84428, Riyadh 11671, Saudi Arabia
[2] Department of Chemistry, College of Science, Imam Mohammad Ibn Saud Islamic University (IMSIU), Riyadh 11623, Saudi Arabia
[3] Chemistry Department, Faculty of Science, Benha University, Benha 13518, Egypt
[4] Chemistry Department, Faculty of Science, Sudan University of Science and Technology (SUST), P.O. Box 407, Khartoum 13311, Sudan
* Correspondence: eaaahmed@imamu.edu.sa or dr.ehabsaleh@yahoo.com

Abstract: In this work, amorphous and crystalline novel products based on Zr, Mg, and Mn were facilely fabricated through the Pechini sol–gel procedure using inexpensive chemicals and an uncomplicated apparatus. Also, these products showed high efficiency as novel adsorbents in getting rid of basic fuchsin dye from aqueous solutions. The adsorbent, which was fabricated before calcination, was abbreviated as KE. In addition, the adsorbents, which were created at 500 and 700 °C, were designated as KE500 and KE700, respectively. The created adsorbents were characterized using high-level transmission electron microscopy (HR-TEM), X-ray diffraction (XRD), energy dispersive X-ray spectroscopy (EDS), N_2 adsorption/desorption analyzer, and field emission scanning electron microscope (FE-SEM). The XRD showed that the KE adsorbent is amorphous, whereas the KE500 and KE700 adsorbents are mixtures of ZrO_2, $MgMn_2O_4$, and $Mg(Mg_{0.333}Mn_{1.333})O_4$ nanostructures. The HR-TEM exhibited that the KE adsorbent consists of very fine irregular shapes, whereas the KE500 adsorbent contains quasi-spherical particles with a mean diameter of 45.16 nm. Furthermore, the HR-TEM exhibited that the KE700 adsorbent consists of polyhedral shapes with a mean diameter of 76.28 nm. Furthermore, the BET surface area of the KE, KE500, and KE700 adsorbents is 67.85, 20.15, and 13.60 m^2/g, respectively. Additionally, the elimination of basic fuchsin dye by the KE, KE500, and KE700 adsorbents is exothermic, physical in nature, and follows the pseudo-first-order as well as Langmuir equations. Further, the maximum uptake capabilities of the KE, KE500, and KE700 adsorbents toward basic fuchsin dye are 239.81, 174.83, and 93.19 mg/g, respectively.

Keywords: nanostructures; adsorption; basic fuchsin dye; analytical parameters

check for updates

Citation: Al-Wasidi, A.S.; Khairy, M.; Abdulkhair, B.Y.; Abdelrahman, E.A. Efficient Disposal of Basic Fuchsin Dye from Aqueous Media Using $ZrO_2/MgMn_2O_4/Mg(Mg_{0.333}Mn_{1.333})O_4$ as a Novel and Facilely Synthesized Nanocomposite. *Inorganics* **2023**, *11*, 363. https://doi.org/10.3390/inorganics11090363

Academic Editor: Paolo Fornasiero

Received: 15 August 2023
Revised: 30 August 2023
Accepted: 5 September 2023
Published: 7 September 2023

1. Introduction

In recent years, people have complained about the scarcity of natural water resources, prompting experts to seek out secure alternatives. Some industries, such as textiles, paints, and pigments, utilize large quantities of water. These large quantities of dye-bearing water are dispersed into the environment in one way or another, leading to environmental contamination and the spread of numerous diseases among the local population [1–5]. Utilizing advanced oxidation processes, photocatalytic degradation, membrane filtration, enzyme degradation, coagulation/flocculation, and adsorption techniques [6–15], organic dyes have been decontaminated. Among these approaches, the adsorption technique was widely utilized as a cost-effective and simple procedure for water remediation [16–21]. Basic fuchsin dye (BFD), also known as basic violet 14, is a cationic dye exploited to color textile, leather, and silk products. Moreover, it is anesthetic, fungicidal, and bactericidal.

It is non-biodegradable and toxic, and hence this dye causes environmental pollution when discharged into water [22]. Khan et al. synthesized iron-manganese-oxide-coated kaolinite for the removal of BFD dye, where the uptake capability was 10.36 mg/g [23]. Ai et al. synthesized an activated carbon/ferrospinel composite for the removal of BFD dye, where the uptake capability was 101mg/g [24]. Hinojosa-Reyes et al. synthesized hydrogen titanate nanotubes for the elimination of BFD dye, where the uptake capability was 183.2 mg/g [25]. Apostol et al. synthesized adsorbent based on xanthan and a ferrite/lignin hybrid for the removal of BFD dye, where the uptake capability was 33.33 mg/g [26]. Nanomaterials, such as zinc oxide, aluminum oxide, Fe_3O_4, and MgO, are highly efficient in removing pollutants owing to their small crystal size and great BET surface area [27–30]. The Pechini sol–gel method has succeeded in obtaining many nanomaterials such as $Li_2B_4O_7/NiO/Ni_3(BO_3)_2$ nanocomposites, SiO_2, MgO, Cu_2O/Li_3BO_3 nanocomposites, Fe_2O_3, and MgO/Y_2O_3 [31–35]. In this method, chelates are formed between cations and hydroxycarboxylic acids, such as citric acid. After that, esterification occurs through the interaction of the carboxylic group of citric acid with the hydroxyl group of ethylene glycol to produce a three-dimensional network. Moreover, the solvent is evaporated, and the resulting gel is calcinated at a moderate temperature to get rid of the organic part and obtain nanomaterials [16]. So, in the present work, amorphous and crystalline novel adsorbents based on Zr, Mg, and Mn were facilely created using the Pechini sol–gel procedure for the efficient disposal of basic fuchsin dye from aqueous solutions. The effects of pH, contact time, temperature, and initial basic fuchsin dye concentration were also investigated. The synthesis of the $ZrO_2/MgMn_2O_4/Mg(Mg_{0.333}Mn_{1.333})O_4$ nanocomposite presents numerous benefits, positioning it as a highly promising option for water treatment applications. Through the strategic integration of these three constituents, a cooperative phenomenon arises that amplifies the nanocomposite's overall functionality. The inclusion of ZrO_2, $MgMn_2O_4$, and $Mg(Mg_{0.333}Mn_{1.333})O_4$ within the nanocomposite structure results in an increased availability of active sites for adsorption. This amalgamation leads to an elevated adsorption capacity, consequently enabling a more effective extraction of basic fuchsin dye from aqueous environments. The collaborative influence among these elements serves to augment the comprehensive adsorption performance of the nanocomposite.

2. Experimental

2.1. Chemicals

Zirconyl chloride octahydrate ($ZrOCl_2{\cdot}8H_2O$), sodium hydroxide (NaOH), manganese(II) acetate tetrahydrate ($Mn(CH_3COO)_2{\cdot}4H_2O$), citric acid ($C_6H_8O_7$), magnesium nitrate hexahydrate ($Mg(NO_3)_2{\cdot}6H_2O$), hydrochloric acid (HCl), potassium chloride (KCl), ethylene glycol ($C_2H_6O_2$), and basic fuchsin dye ($C_{20}H_{19}N_3{\cdot}HCl$) were of high purity (analytical grade) and acquired from Sigma Aldrich, then utilized without undergoing any purification processes.

2.2. Synthesis of Zr/Mg/Mn/O Adsorbents

In total, 10.00 g of $ZrOCl_2{\cdot}8H_2O$ was dissolved in about 50 mL of deionized water. Also, 7.61 g of $Mn(CH_3COO)_2{\cdot}4H_2O$ was dissolved in about 50 mL of deionized water. Moreover, 7.96 g of $Mg(NO_3)_2{\cdot}6H_2O$ was also dissolved in about 50 mL of deionized water. The three metallic solutions were then combined and magnetically agitated at 550 rpm for 15 min. Moreover, the citric acid solution, which was freshly prepared through dissolving 17.89 g of citric acid in about 50 mL of deionized water, was slowly added and then the produced mixture was subjected to magnetic stirring at 550 rpm for 15 min. Furthermore, 12 mL of ethylene glycol was slowly added, and then the produced mixture was subjected to magnetic stirring at 550 rpm at 150 °C till dryness. Additionally, the generated powder was then calcined in a muffle at 500 and 700 °C for 5 h. The samples that were obtained at 500 and 700 °C were designated as KE500 and KE700, respectively. In addition, the sample that was obtained before calcination was abbreviated as KE.

2.3. Characterization of the Synthesized Adsorbents

Patterns of X-ray diffraction (XRD) of the KE, KE500, and KE700 samples were obtained at room temperature, applying a Bruker D8 Advance diffractometer (Billerica, MA, United States) with CuK_α radiation (wavelength = 1.54 Å), a step rate of 0.4 1/min, and a 2θ range of 5°–70°. A field emission scanning electron microscope (FE-SEM) of the JSM-IT800 Schottky model (Akishima, Tokyo, Japan) with coupled energy dispersive X-ray spectroscopy (EDS) was used to acquire images of the surface morphology of the KE, KE500, and KE700 products as well as qualitative and quantitative information on the composition of the synthesized samples. A transmission electron microscope (TEM, Model: Talos F200iS, Waltham, MA, United States) was used to acquire images of the particle morphology of the KE, KE500, and KE700 samples. Through applying a BET surface area analyzer (Quantachrome, Model: TouchWin, Boynton Beach, FL, United States), the pore features in addition to the BET surface areas of the KE, KE500, and KE700 samples were determined.

2.4. Removal of BFD Dye from Aqueous Solutions

For investigating the influence of solution pH in the range of 2.5–8.5, batch removal experiments were accomplished by shaking 50 mg of KE, KE500, or KE700 samples with 100 mL of about 200 mg/L aqueous BFD solution for 180 min. After that, the adsorbent was retracted from the mixture by centrifugation for 3 min at 3500 rpm. After centrifugation, the yielded filtrate was examined at 544 nm, applying a UV–Vis spectrophotometer (Model: Shimadzu 1800) to estimate the equilibrium BFD dye concentration. In addition, the influences of interaction time (5–40 min), interaction temperature (298–328 kelvin), and primary BFD concentration (150–300 mg/L) were also investigated.

The uptake capability of the KE, KE500, and KE700 adsorbents (U, mg/g) and the uptake efficacy of BFD dye (% *R*) were calculated by applying Equations (2) and (1), respectively [36].

$$\% R = \frac{E_o - E_e}{E_o} \times 100 \quad (1)$$

$$U = (E_o - E_e) \times \frac{V}{W} \quad (2)$$

E_o and E_e are the original and equilibrium BFD dye concentrations (mg/L), respectively. In addition, *W* and *V* are the quantity of adsorbent sample (g) and the volume of BFD dye solution (L), respectively.

The procedure described by Khalifa et al. [12] was employed to determine the point of zero charge (pH_{PZC}) for the KE, KE500, and KE700 adsorbents. The process involved introducing 0.20 g of either KE, KE500, or KE700 adsorbents into separate 0.05 L solutions of 0.026 M KCl. Additionally, the initial pH ($pH_{Initial}$) of the utilized KCl solutions was systematically adapted within the 2.50–11.50 range. Each mixture of adsorbent and KCl was continuously stirred for 6 hrs. Subsequently, the resulting pH values (pH_{Final}) were ascertained and plotted against their corresponding initial pH values ($pH_{Initial}$). The pH_{Final} value corresponding to the point on the plot where a clear plateau emerged was designated as the pH_{pzc}.

3. Results and Discussion

3.1. Characterization of the Fabricated Products

3.1.1. XRD

Figure 1A–C illustrates the XRD patterns of the KE, KE500, and KE700 samples, respectively. Additionally, the obtained results exhibited that the KE product is amorphous due to the broad peaks at 2θ = 28° and 50°. In addition, the KE500 and KE700 samples consist of zirconium oxide (ZrO_2), magnesium manganese oxide ($MgMn_2O_4$), and magnesium manganese oxide ($Mg(Mg_{0.333}Mn_{1.333})O_4$)), as obtained from JCPDS Nos. 00-065-0729, 00-023-0392, and 00-062-0483, respectively. The crystal system, space group, and lattice

volume of ZrO_2 are tetragonal, P42/nmc (137), and 67.12 Å^3, respectively. Also, the crystal system, space group, and lattice volume of $MgMn_2O_4$ are tetragonal, I41/amd (141), and 306.64 Å^3, respectively. Moreover, the crystal system, space group, and lattice volume of $Mg(Mg_{0.333}Mn_{1.333})O_4$ are cubic, Fd-3m (227), and 570.20 Å^3, respectively. The peaks at 2θ = 30.45°, 35.47°, 50.91°, and 60.45° correspond to the (101), (110), (200), and (211) miller planes of ZrO_2, respectively. The peaks at 2θ = 18.29°, 32.71°, 38.70°, 44.72°, 60.54°, and 65.11° correspond to the (101), (103), (004), (220), (224), and (400) miller planes of $MgMn_2O_4$, respectively. The peaks at 2θ = 43.77°, 57.54°, and 63.12° correspond to the (400), (511), and (440) miller planes of $Mg(Mg_{0.333}Mn_{1.333})O_4$, respectively. The average crystallite size, which was estimated using the Scherrer equation, of the KE500 and KE700 samples was 38.27 and 70.45 nm, respectively.

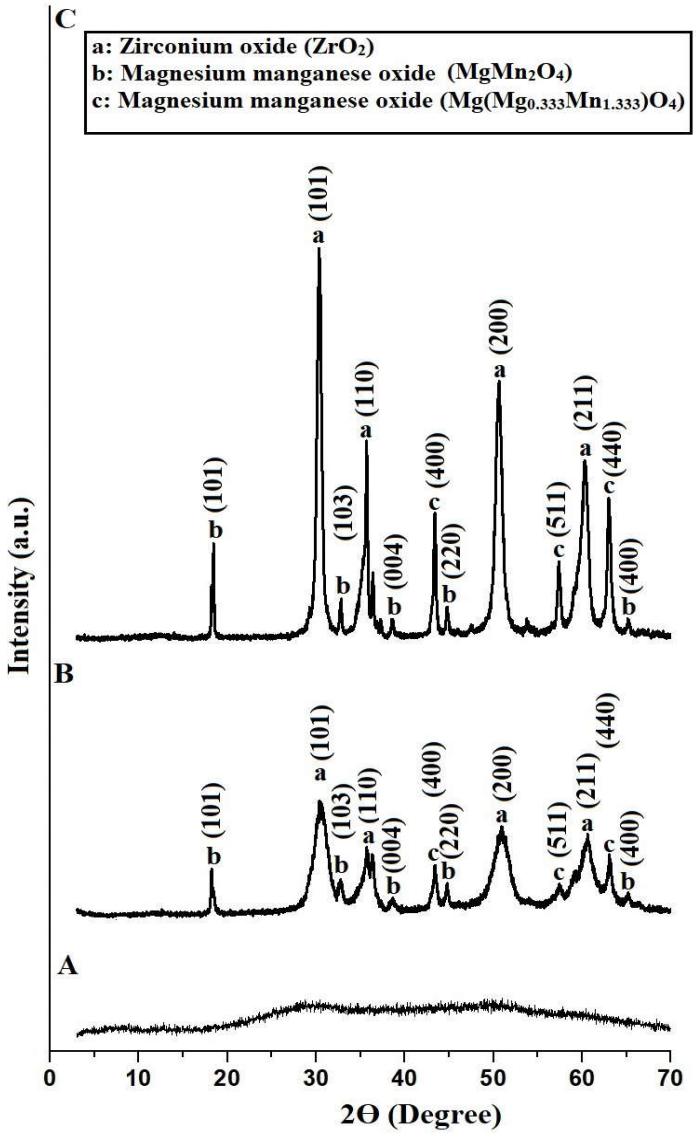

Figure 1. X-ray Diffraction Patterns of the KE (**A**), KE500 (**B**), and KE700 (**C**) products.

3.1.2. EDS

Figure 2A–C illustrates the EDS patterns of the KE, KE500, and KE700 products, respectively. Furthermore, the obtained findings exhibited that the KE and KE500 products are composed of C, Mg, Zr, Mn, and O, as revealed in Table 1. Moreover, the presence of carbon in those samples was due to the incomplete burning of citric acid. In addition, the KE700 sample was composed of Mg, Zr, Mn, and O, as revealed in Table 1. Therefore, 700 °C was sufficient to make the citric acid burn completely.

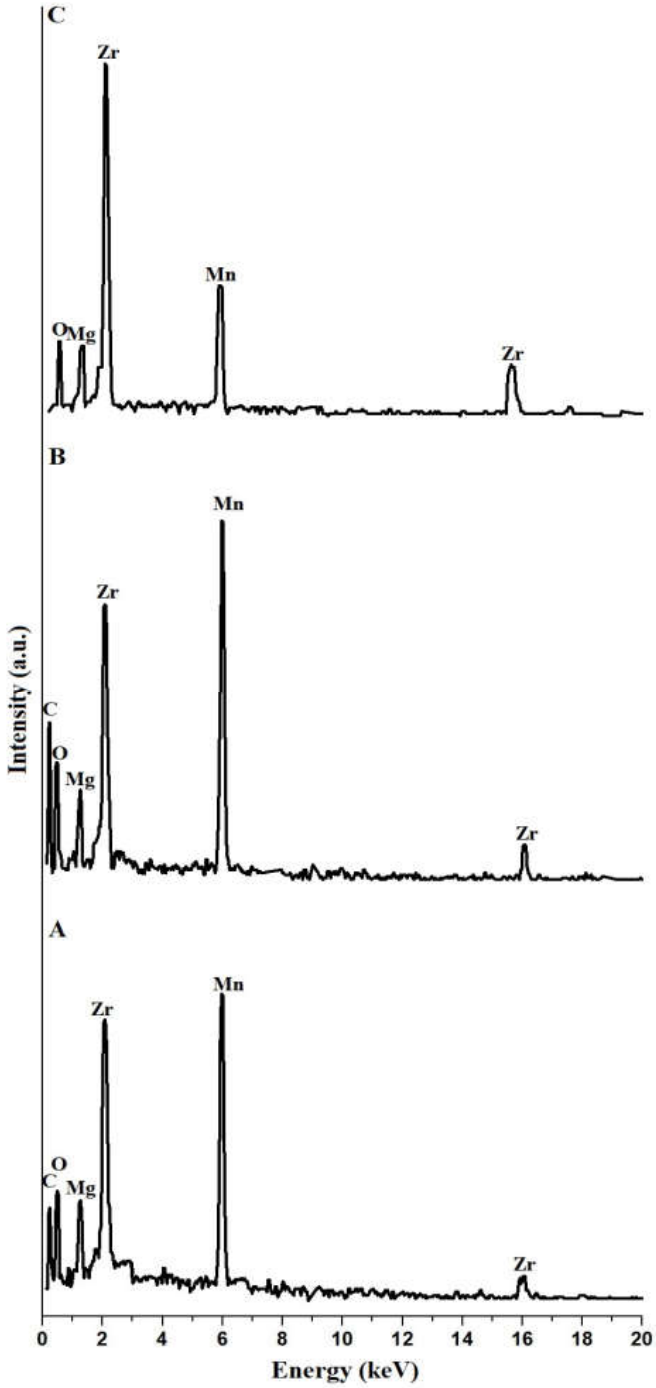

Figure 2. EDS patterns of the KE (**A**), KE500 (**B**), and KE700 (**C**) products.

Table 1. Elements and their percentages in the KE, KE500, and KE700 samples.

Samples	% C	% O	% Mg	% Mn	% Zr
KE	36.25	28.47	4.70	11.78	18.80
KE500	33.96	23.84	5.98	13.77	22.45
KE700	----	18.22	9.28	14.14	58.36

3.1.3. FE-SEM and HR-TEM

Figure 3A–C illustrates the FE-SEM pictures of the KE, KE500, and KE700 samples, respectively. Additionally, the findings exhibited that the KE product consists of very fine

irregular shapes. In addition, the KE500 product contains quasi-spherical particles with a mean grain size of 90.26 nm. Further, the KE700 product is composed of polyhedral shapes with a mean grain size of 650 nm. Figure 4A–C represents the high-resolution transmission electron microscopy (HR-TEM) pictures of the KE, KE500, and KE700 products, respectively. In addition, the findings exhibited that the KE product consists of very fine irregular shapes. Additionally, the KE500 product contains quasi-spherical particles with a mean diameter of 45.16 nm. Furthermore, the KE700 product consists of polyhedral shapes with a mean diameter of 76.28 nm.

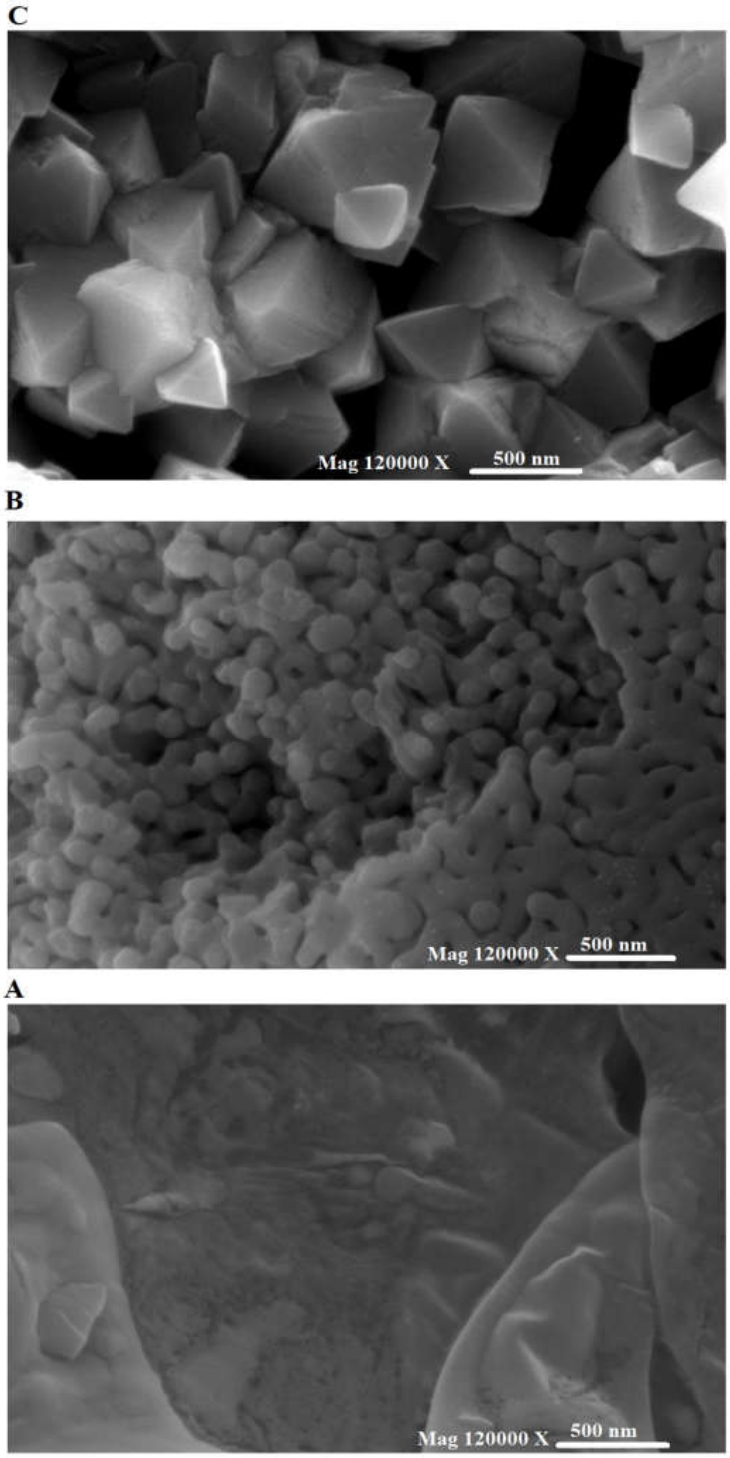

Figure 3. FE-SEM pictures of the KE (**A**), KE500 (**B**), and KE700 (**C**) products.

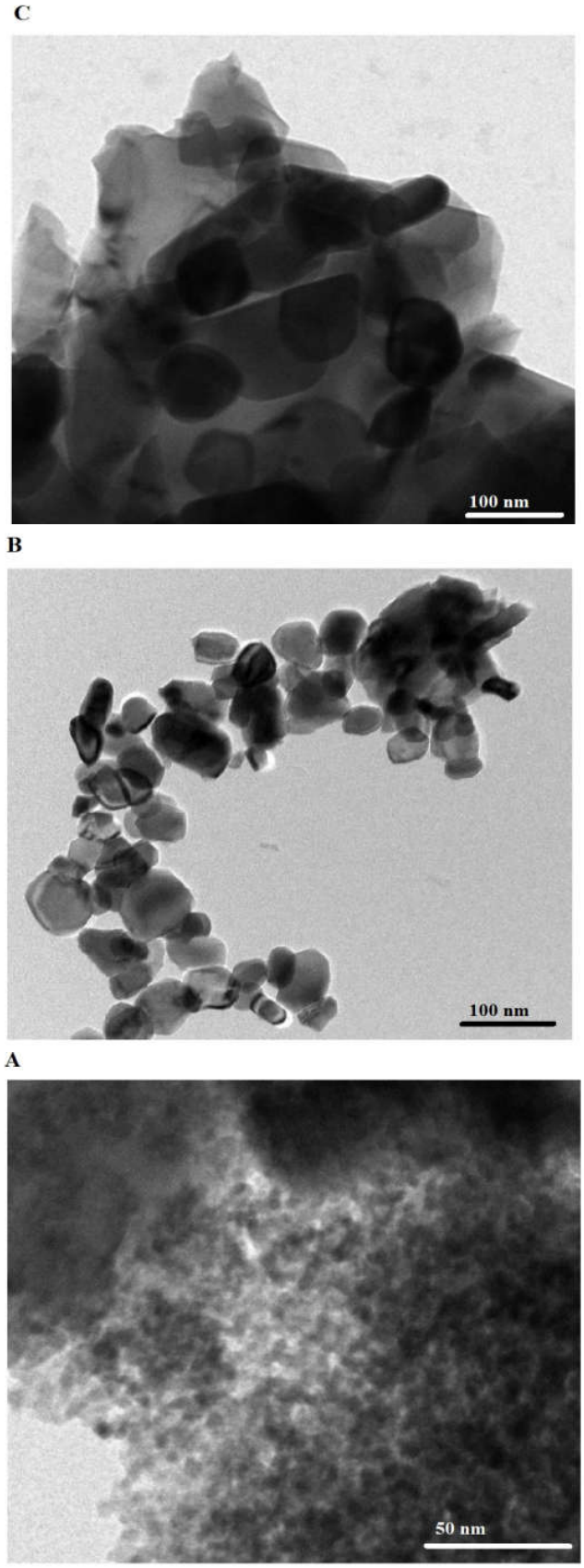

Figure 4. HR-TEM pictures of the KE (**A**), KE500 (**B**), and KE700 (**C**) products.

3.1.4. Nitrogen Adsorption/Desorption

Figure 5A–C illustrates the nitrogen adsorption/desorption curves of the KE, KE500, and KE700 products, respectively. Furthermore, the obtained findings confirmed that the isotherms correspond to the IV-type isotherm, which shows the mesoporous nature of the products [16]. The surface textures, for example, BET surface area, average pore size, and total pore volume, are listed in Table 2. It was found that the BET surface area rises according to the following order, KE > KE500 > KE700, owing to the inverse relationship between surface area and crystalline size.

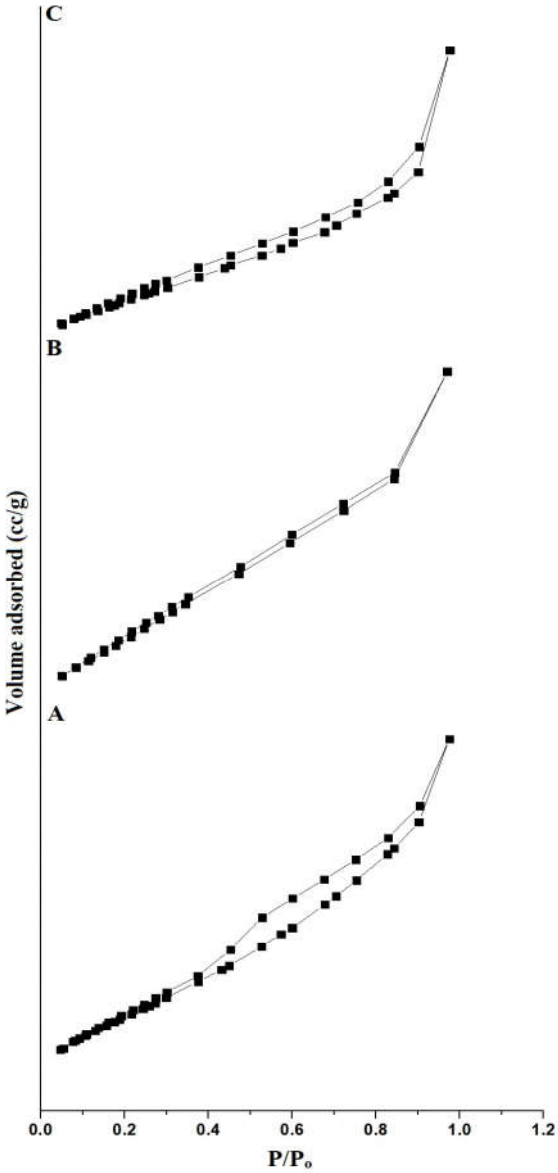

Figure 5. The nitrogen adsorption/desorption isotherm of KE (**A**), KE500 (**B**), and KE700 (**C**) samples.

Table 2. Surface characteristics of the KE, KE500, and KE700 products.

Sample	BET Surface Area (m^2/g)	Total Pore Volume (cc/g)	Average Pore Size (nm)
KE	67.85	0.1077	3.17
KE500	20.15	0.0265	2.63
KE700	13.60	0.0305	4.49

3.2. Removal of BFD Dye from Aqueous Media

3.2.1. Effect of pH

Figure 6A,B illustrates the effect of solution pH on the uptake efficacy of BFD dye as well as the uptake capability of the KE, KE500, and KE700 products, respectively. It was observed that the uptake efficacy of BFD dye and the uptake capability of the KE, KE500, and KE700 products increased with rising pH from 2.50 to 8.50. The uptake efficacy of BFD dye using the KE, KE500, and KE700 adsorbents at pH 8.5 is 56.36, 38.82, and 19.84%, respectively. In addition, the uptake capability of the KE, KE500, and KE700 adsorbents at pH 8.5 is 225.42, 155.26, and 79.36 mg/g, respectively.

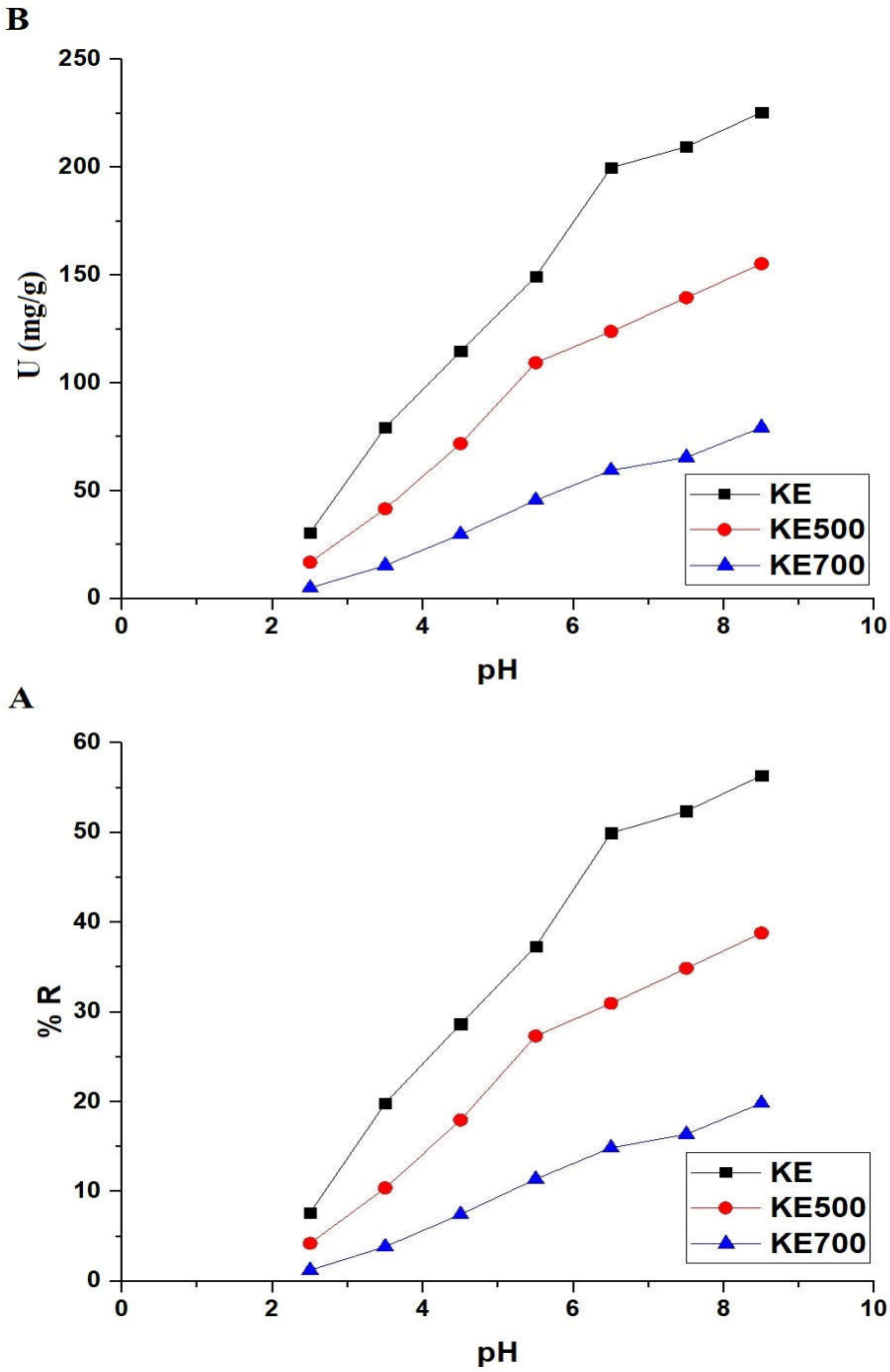

Figure 6. The influence of solution pH on uptake efficacy of BFD dye (**A**) and uptake capability of the KE, KE500, and KE700 adsorbents (**B**).

To clarify the adsorption process, the KE sample was photographed (as an illustrative example) before and after adsorption at pH 8, as shown in Figure 7. As is clear from the figure, the color intensity decreased significantly after adsorption.

Figure 7. Image of the BFD dye before and after the adsorption process at pH 8 using KE as an adsorbent.

In addition, the point of zero charge (pH_{PZC}) of the KE, KE500, and KE700 products is represented in Figure 8. The point of zero charge (pH_{PZC}) of the KE, KE500, and KE700 adsorbents is 5.10, 5.31, and 5.60, respectively. If pH < pH_{PZC}, the medium works to surround the surface of the KE, KE500, and KE700 adsorbents with positive hydrogen ions that are repellent with positively charged BFD dye, as displayed in Scheme 1, and hence reduce the uptake efficacy and uptake capability [16]. If pH > pH_{PZC}, the medium works to surround the surface of the KE, KE500, and KE700 adsorbents with negative hydroxide ions that attract the positively charged BFD dye, as displayed in Scheme 1, and hence enhance the uptake efficacy and uptake capability [16].

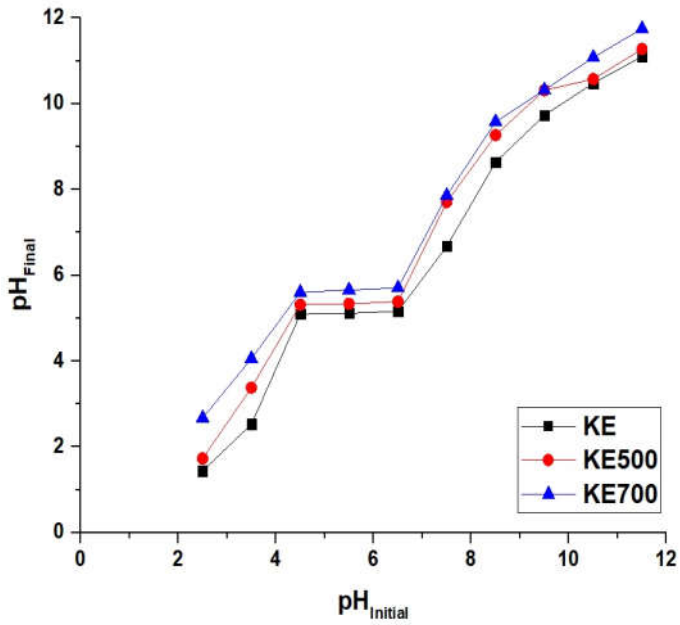

Figure 8. Point of zero charge (pH_{PZC}) of the KE, KE500, and KE700 products.

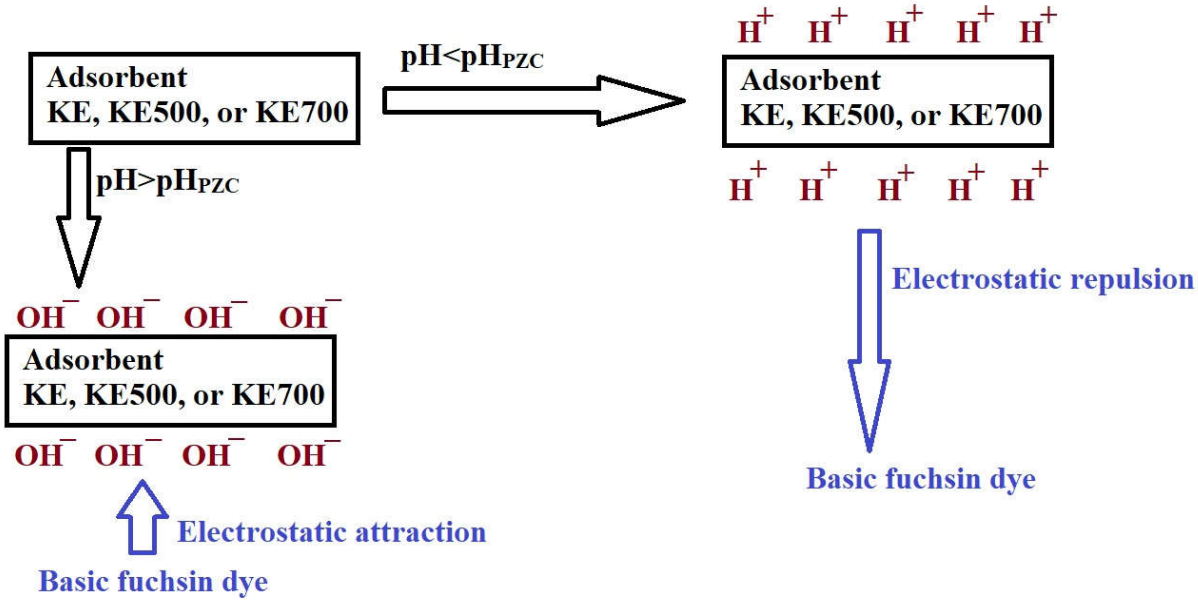

Scheme 1. Removal mechanism of basic fuchsin dye using the KE, KE500, and KE700 adsorbents.

In order to study the stability of the KE, KE500, and KE700 samples at different pH values (2.5–8.5), the XRD of the synthesized adsorbents was carried out at these pH values (figures omitted for brevity). The results showed that there is no difference in the intensity or locations of the XRD peaks, which confirms their stability. Additionally, the inductively coupled plasma analysis revealed that there is no release of ions from the KE, KE500, or KE700 adsorbents into the filtrate while undergoing adsorption. As a result, the safety of the synthesized adsorbents is established, allowing their application in water pollution treatment.

3.2.2. Effect of Interaction Time

Figure 9A,B illustrates the influence of interaction time on the uptake efficacy of basic fuchsin dye as well as the uptake capability of the KE, KE500, and KE700 products, respectively. It was observed that the uptake efficacy of basic fuchsin dye and the uptake capability of the KE, KE500, and KE700 products increased with rising interaction time from 5 to 30 min. In addition, stability was observed in these parameters when the time was increased from 30 to 40 min due to the saturation of the adsorption sites. The uptake efficacy of basic fuchsin dye using the KE, KE500, and KE700 adsorbents after 30 min was 57.36, 39.88, and 19.24%, respectively. In addition, the uptake capability of the KE, KE500, and KE700 adsorbents after 30 min was 229.44, 159.50, and 76.96 mg/g, respectively.

The pseudo-second-order (Equation (4)) and the pseudo-first-order (Equation (3)) kinetic models [16] were operated to study the linear fitting of the obtained experimental results owing to the elimination of BFD dye using the KE, KE500, and KE700 adsorbents, as displayed in Figure 10A,B, respectively.

$$\log(U_e - U_t) = logU_e - \frac{k_1}{2.303}t \quad (3)$$

$$\frac{t}{U_t} = \frac{1}{k_2 U_e^2} + \frac{1}{U_e}t \quad (4)$$

where k_1 is the pseudo-first-order rate constant (1/min), U_t is the amount of BFD dye adsorbed at time t (mg/g), k_2 is the pseudo-second-order rate constant (g/mg.min), and U_e is the quantity of BFD dye adsorbed at equilibrium (mg/g). The resulting constants and the correlation coefficients (R^2) are displayed in Table 3. In addition, the removal of BFD dye using the KE, KE500, and KE700 products obeys the pseudo-first-order due to

the following reasons: (1) The R^2 values for the pseudo-first-order exhibit greater values compared to the R^2 values for the pseudo-second-order. (2) The calculated U_e values from the pseudo-first-order closely align with the experimental U_e values.

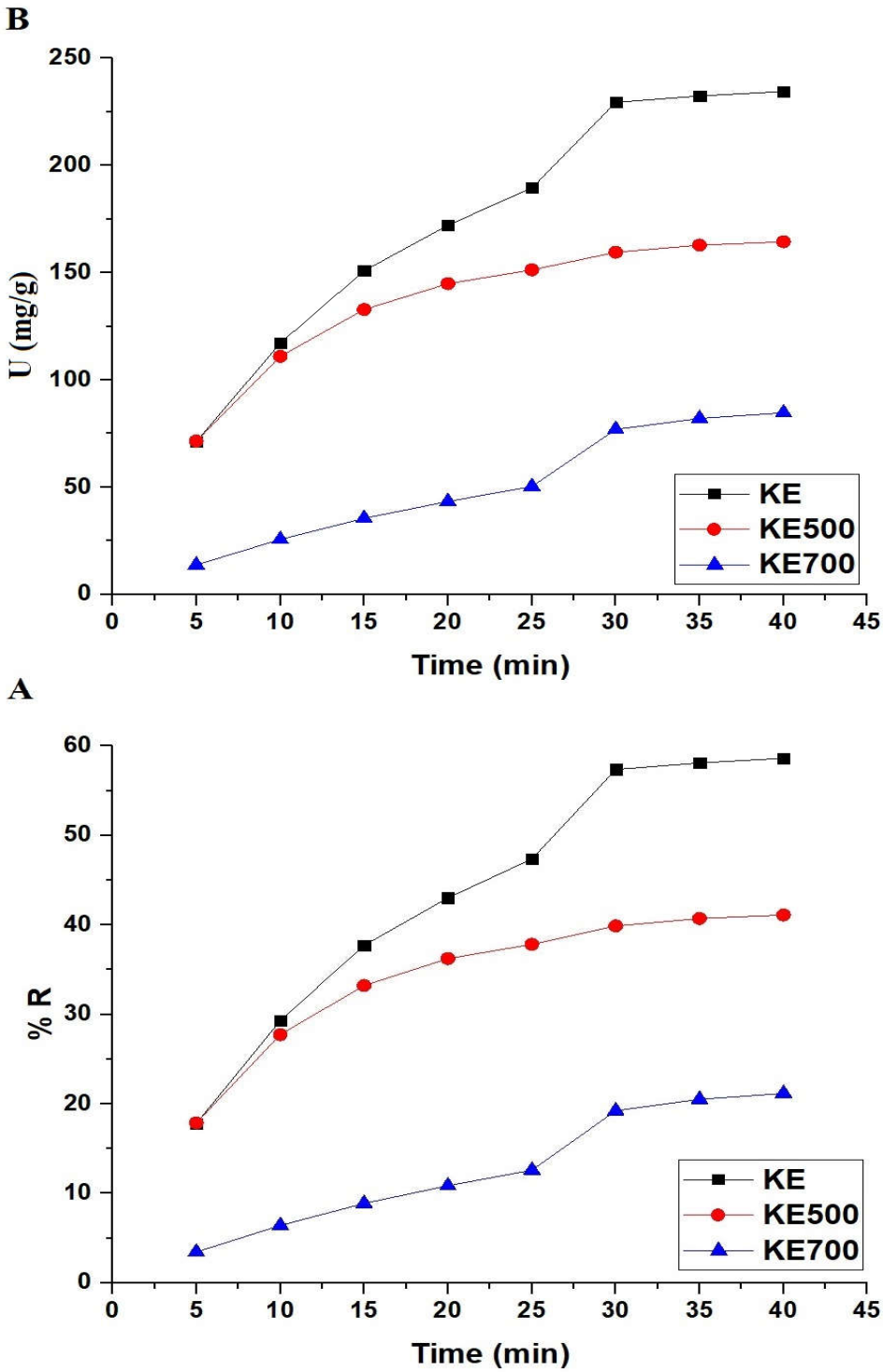

Figure 9. The impact of interaction time on uptake efficacy of BFD dye (**A**) and uptake capability of the KE, KE500, and KE700 adsorbents (**B**).

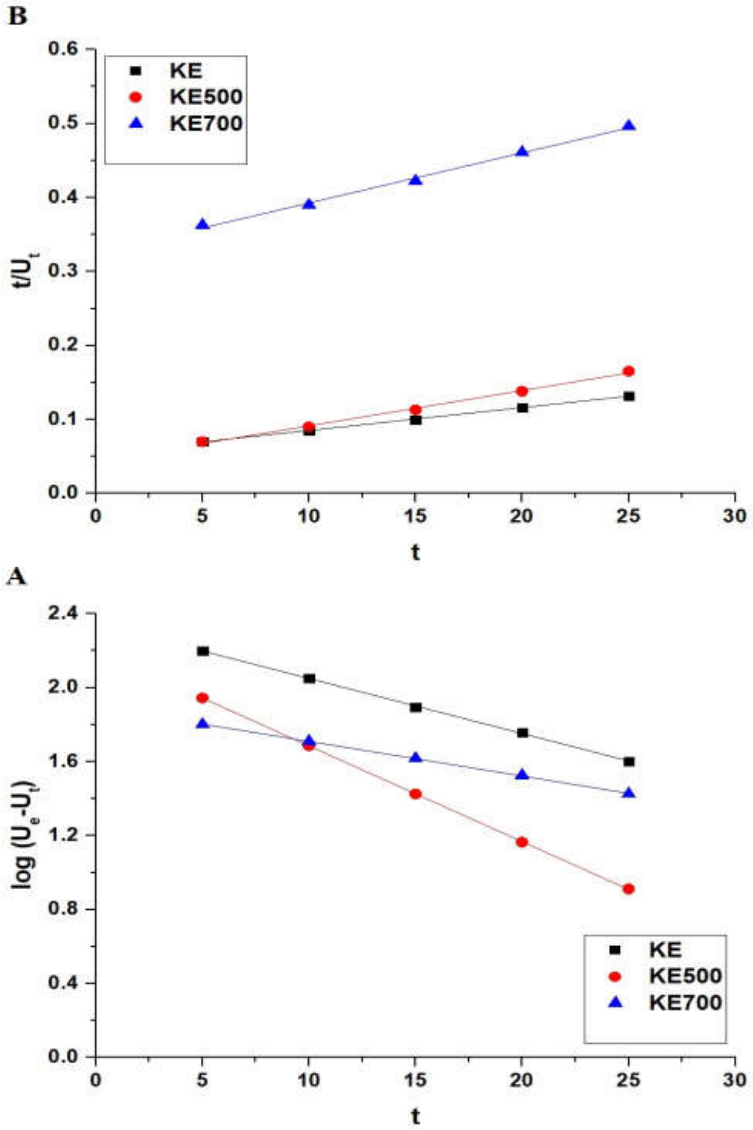

Figure 10. Plot of log (U_e-U_t) (**A**) and t/U_t (**B**) versus t for the disposal of BFD dye by the KE, KE500, and KE700 adsorbents.

Table 3. Kinetic constants for the disposal of BFD dye by the KE, KE500, and KE700 adsorbents.

Adsorbent	Pseudo-First-Order			Pseudo-Second-Order		
	k_1 (1/min)	U_e (mg/g)	R^2	k_2 (g/mg.min)	U_e (mg/g)	R^2
KE	0.0685	222.36	0.9996	0.00018	323.62	0.9989
KE500	0.1192	159.33	0.9999	0.00052	209.64	0.9956
KE700	0.0431	78.79	0.9994	0.00014	147.71	0.9945

3.2.3. Effect of Interaction Temperature

Figure 11A,B illustrate the impact of interaction temperature on the uptake efficacy of BFD dye as well as the uptake capability of the KE, KE500, and KE700 products, respectively. It was observed that the uptake efficacy of BFD dye and the uptake capability of the KE, KE500, and KE700 products decreased with rising temperatures from 298 to 328 kelvin. The uptake efficacy of BFD dye using the KE, KE500, and KE700 adsorbents at 328 kelvin is 44.33, 23.52, and 13.55%, respectively. In addition, the uptake capability of the KE, KE500, and KE700 adsorbents at 328 kelvin is 177.30, 94.08, and 54.18 mg/g, respectively.

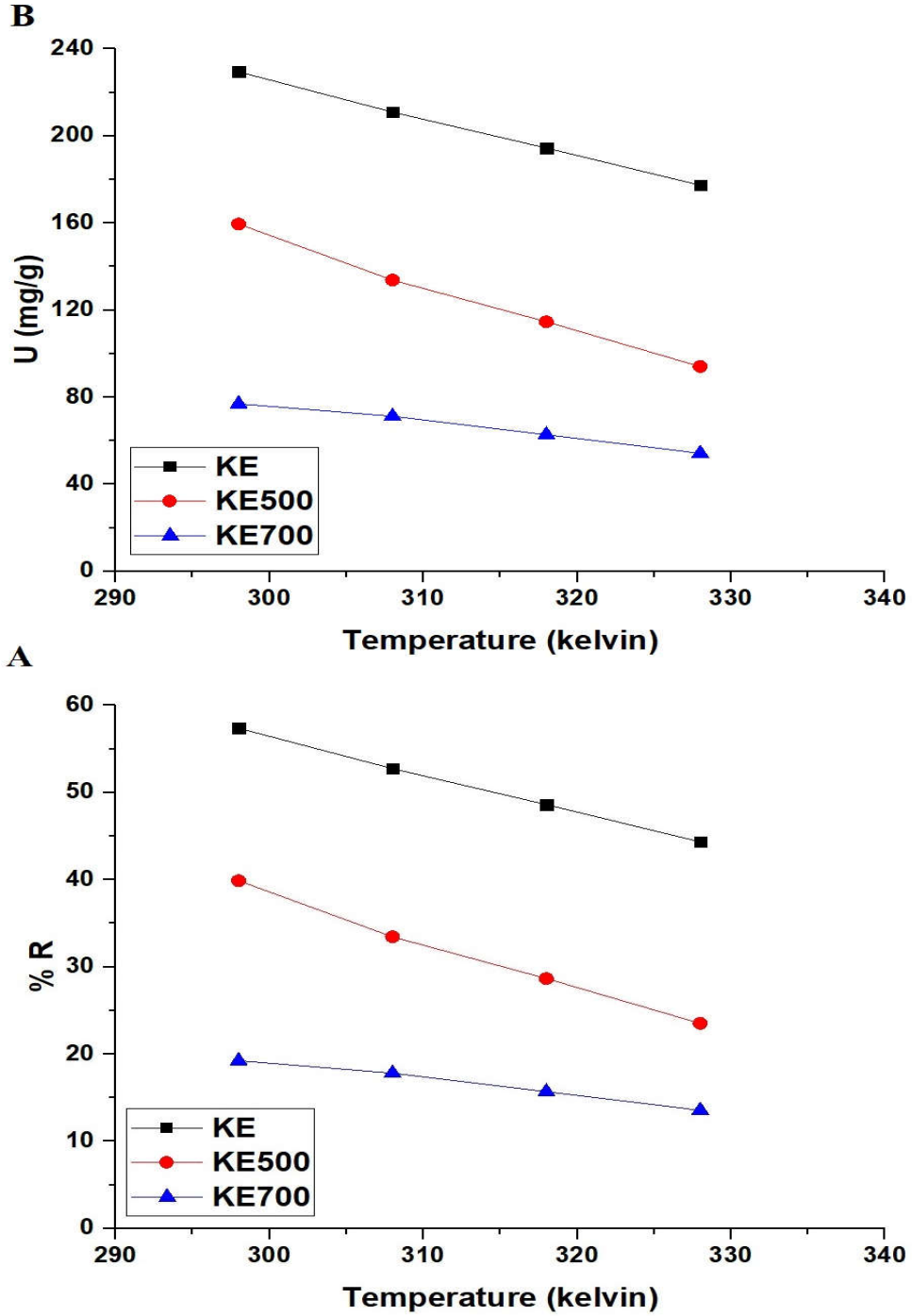

Figure 11. The influence of temperature on uptake efficacy of BFD dye (**A**) and the uptake capability of the KE, KE500, and KE700 adsorbents (**B**).

The impact of solution temperature on the elimination of BFD dye by the KE, KE500, and KE700 adsorbents was investigated by exploiting the thermodynamic constants, for instance, ΔG° (change in free energy, kJ/mol), ΔH° (change in enthalpy, kJ/mol), and ΔS° (change in entropy, kJ/mol kelvin) which were estimated using Equations (5)–(7) [16].

$$\ln K_T = \frac{\triangle S^\circ}{R} - \frac{\triangle H^\circ}{RT} \tag{5}$$

$$\triangle G^\circ = \triangle H^\circ - T \triangle S^\circ \tag{6}$$

$$K_T = \frac{U_e}{E_e} \tag{7}$$

where R is the universal gas constant (kJ/mol kelvin). T is the absolute temperature (kelvin). K_T is the distribution constant (L/g). In addition, the linear alteration of lnK_T versus $1/T$ is displayed in Figure 12, and the thermodynamic constants can be estimated from the intercept and slope. Additionally, the thermodynamic constants for the elimination of BFD dye using the KE, KE500, and KE700 products are displayed in Table 4. Negative ΔG° values suggested that the elimination of BFD dye by the KE, KE500, and KE700 products is spontaneous. Also, the negative ΔH° values suggested that the elimination of BFD dye by the KE, KE500, and KE700 products is exothermic. Additionally, the positive ΔS° values suggested that the elimination of BFD dye by the KE, KE500, and KE700 products was conducted in the direction of growing system randomness. Moreover, the elimination of BFD dye by the KE, KE500, and KE700 products is physical in nature because the ΔH° values are smaller than 40 kJ/mol [16].

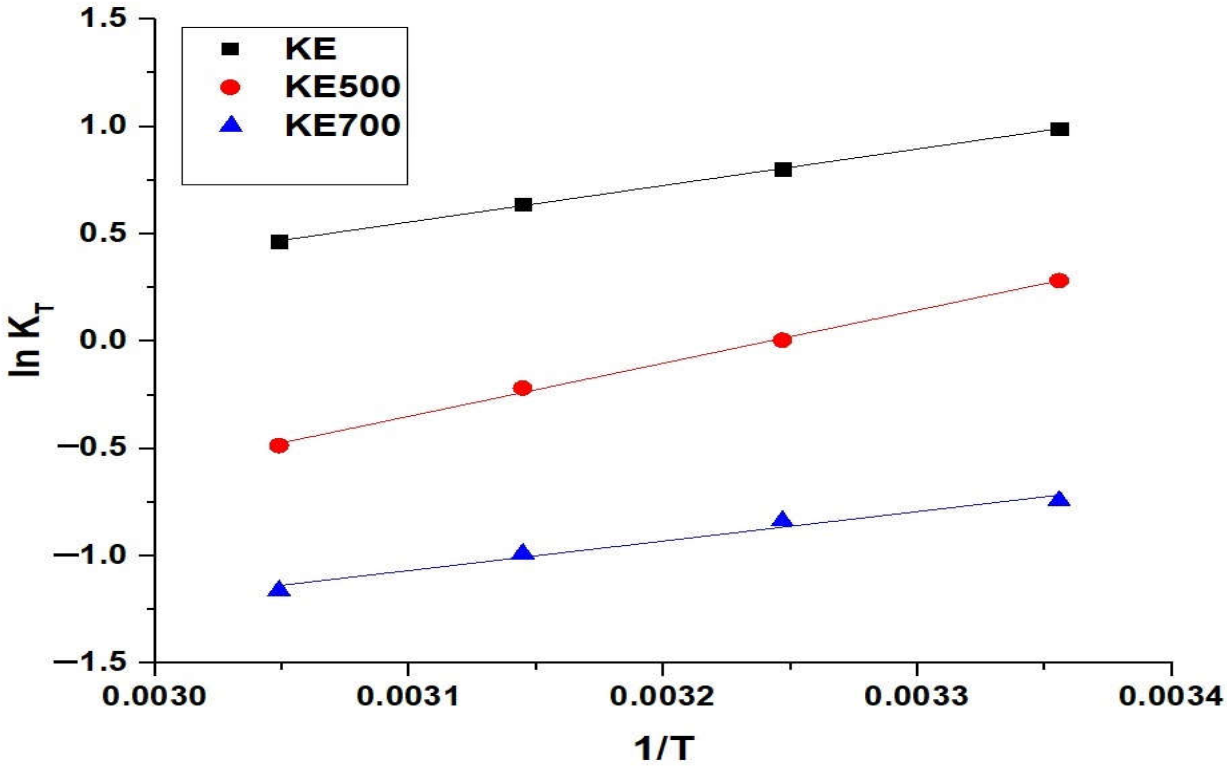

Figure 12. The plot of ln K_T versus 1/T for the disposal of BFD dye by the KE, KE500, and KE700 products.

Table 4. The thermodynamic constants for the elimination of BFD dye by the KE, KE500, and KE700 products.

Adsorbent	ΔH° (kJ/mol)	ΔS° (kJ/mol Kelvin)	ΔG° (kJ/mol)			
			298	308	318	328
KE	−14.20	0.0394	−25.94	−26.34	−26.73	−27.12
KE500	−20.66	0.0669	−40.62	−41.29	−41.96	−42.63
KE700	−11.47	0.0445	−24.73	−25.17	−25.62	−26.06

3.2.4. Effect of BFD Dye Concentration

Figure 13A,B illustrate the impact of the original dye concentration on the uptake efficacy of BFD dye in addition to the uptake capability of the KE, KE500, and KE700 products, respectively. It was found that the uptake efficacy of BFD dye decreased, whereas the uptake capability of the KE, KE500, and KE700 adsorbents increased with increasing initial dye concentrations.

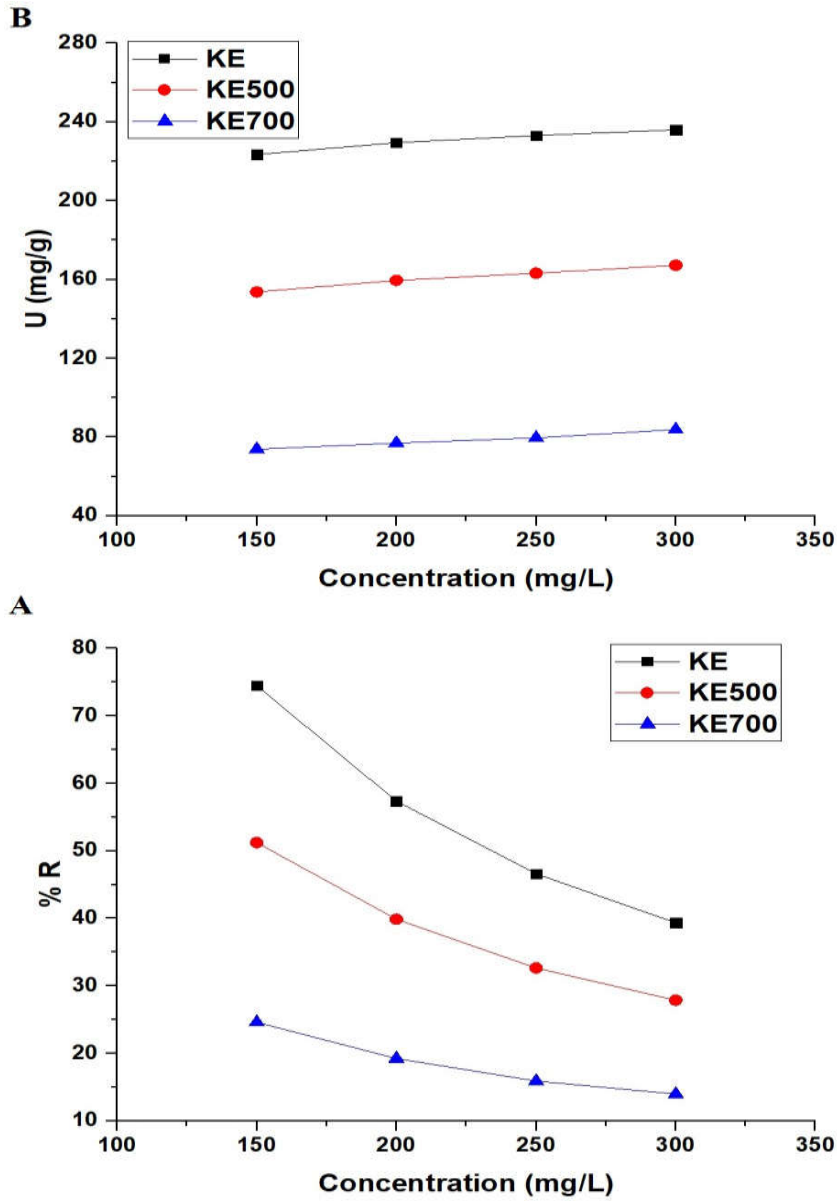

Figure 13. The influence of initial dye concentration on uptake efficacy of BFD dye (**A**) and uptake capability of the KE, KE500, and KE700 adsorbents (**B**).

The Langmuir (Equation (5)) in addition to the Freundlich (Equation (6)) equilibrium equations [16,37–40] were operated to study the linear fitting of the obtained experimental data owing to the disposal of BFD dye by the KE, KE500, and KE700 products, as displayed in Figure 14A,B, respectively.

$$\frac{E_e}{U_e} = \frac{1}{k_3 U_{max}} + \frac{E_e}{U_{max}} \quad (8)$$

$$\ln U_e = \ln k_4 + \frac{1}{x} \ln E_e \tag{9}$$

where $1/x$ represents the heterogeneity constant. k_3 represents the equilibrium constant of the Langmuir isotherm (L/mg). Furthermore, k_4 represents the equilibrium constant of the Freundlich isotherm (mg/g) $(L/mg)^{1/n}$. U_{max} represents the maximum uptake capability of the Langmuir isotherm (mg/g). Further, Equation (7) can be used for determining the U_{max} from the applied Freundlich equilibrium isotherm [16].

$$U_{max} = k_4 \left(E_o^{1/x} \right) \tag{10}$$

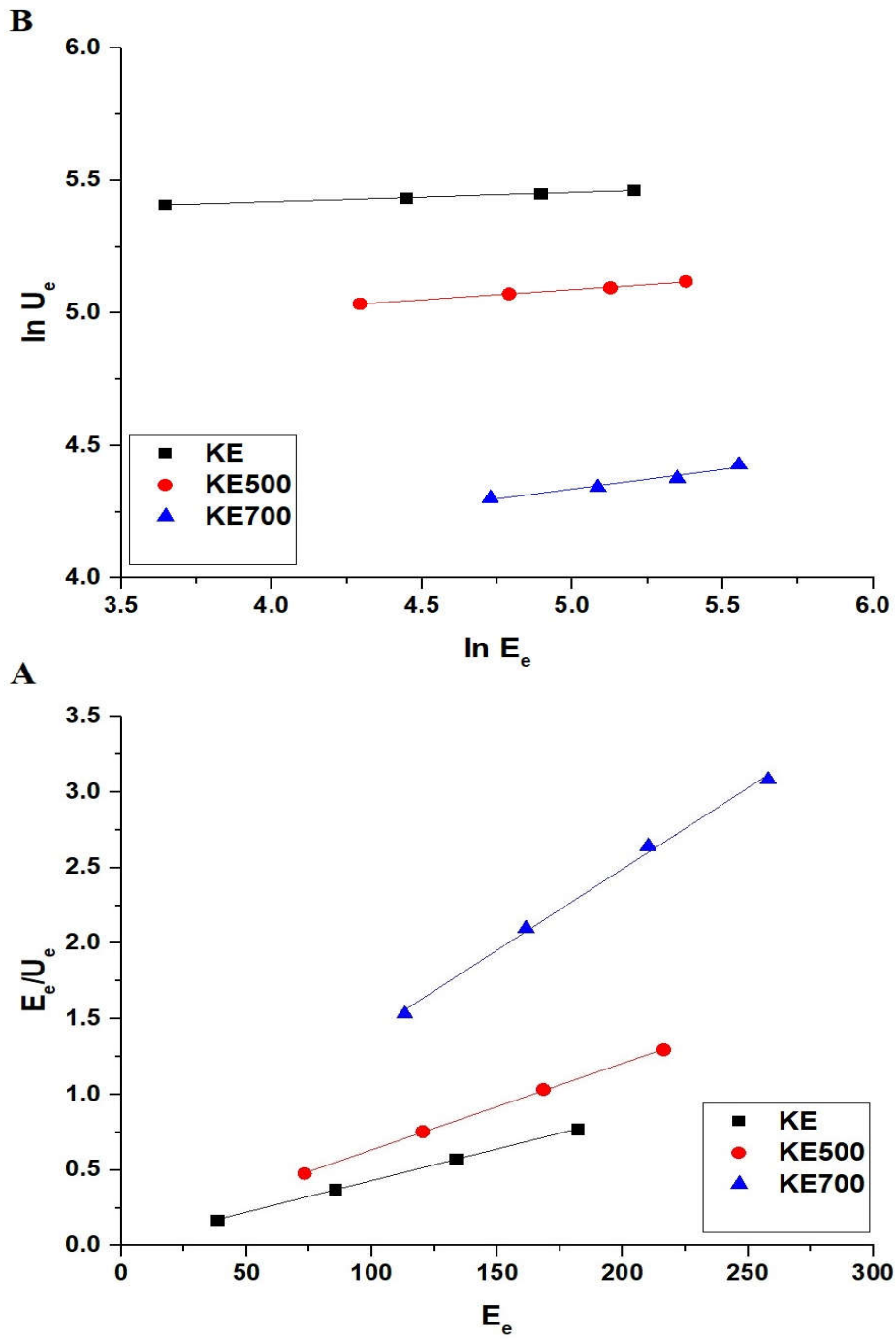

Figure 14. Langmuir (**A**) and Freundlich (**B**) plots for the elimination of BFD dye by the KE, KE500, and KE700 adsorbents.

The resulting constants and the correlation coefficients (R^2) are displayed in Table 5. In addition, the disposal of BFD dye by the KE, KE500, and KE700 products obeys the Langmuir equation because the R^2 values of the Langmuir equation are higher than the R^2 values of the Freundlich equation. Additionally, the maximum uptake capability of the KE, KE500, and KE700 products towards BFD dye is 239.81, 174.83, and 93.19 mg/g, respectively.

Table 5. The obtained equilibrium constants of the disposal of BFD dye by the KE, KE500, and KE700 products.

	Langmuir Isotherm			Freundlich Isotherm		
Adsorbent	**U_{max} (mg/g)**	**k_3 (L/mg)**	**R^2**	**U_{max} (mg/g)**	**k_4 (mg/g) (L/mg)$^{1/n}$**	**R^2**
KE	239.81	0.3064	0.9999	236.49	196.81	0.9979
KE500	174.83	0.0917	0.9996	165.81	110.75	0.9944
KE700	93.19	0.0311	0.9966	79.84	36.53	0.9495

Furthermore, the uptake capability of the KE, KE500, and KE700 samples for adsorbing BFD dye surpassed that of other adsorbents, as evidenced in Table 6. The utilization of $ZrO_2/MgMn_2O_4/Mg(Mg_{0.333}Mn_{1.333})O_4$ as an adsorbent offers several advantages. The combination of these components creates a synergistic influence that increases the overall adsorption operation. This nanocomposite configuration imparts a larger number of active uptake positions, leading to increased uptake capability. Consequently, this composite exhibits a heightened efficiency in removing basic fuchsin dye from aqueous media. The strategic integration of ZrO_2, $MgMn_2O_4$, and $Mg(Mg_{0.333}Mn_{1.333})O_4$ enhances the adsorption potential, making it an excellent choice for water pollution treatment applications.

Table 6. Comparison study between maximum adsorption capabilities of the fabricated adsorbents and those of other adsorbents in the literature for the disposal of BFD dye by the KE, KE500, and KE700 adsorbents [23–26].

Adsorbent	Maximum Uptake Capability (mg/g)	Ref
Iron-manganese-oxide-coated kaolinite	10.36	[23]
Activated carbon/ferrospinel composite	101.00	[24]
Hydrogen titanate nanotubes	183.20	[25]
Xanthan/ferrite/lignin hybrid	33.33	[26]
KE	239.81	This study
KE500	174.83	This study
KE700	93.19	This study

3.2.5. Impact of Desorption and Reusability

The KE, KE500, and KE700 products were renewed by exposure to stirring at 60 °C for 20 min in 50 mL of 1 M HCl, which completely removed the BFD dye from them. Afterward, the regenerated products were utilized for five repeated cycles to eliminate the BFD dye, adhering to the previously outlined experimental steps. According to Figure 15, it can be observed that the percentage of BFD dye removal using the synthesized adsorbents remained relatively stable. This suggests that these products can be employed several times without experiencing a substantial reduction in effectiveness.

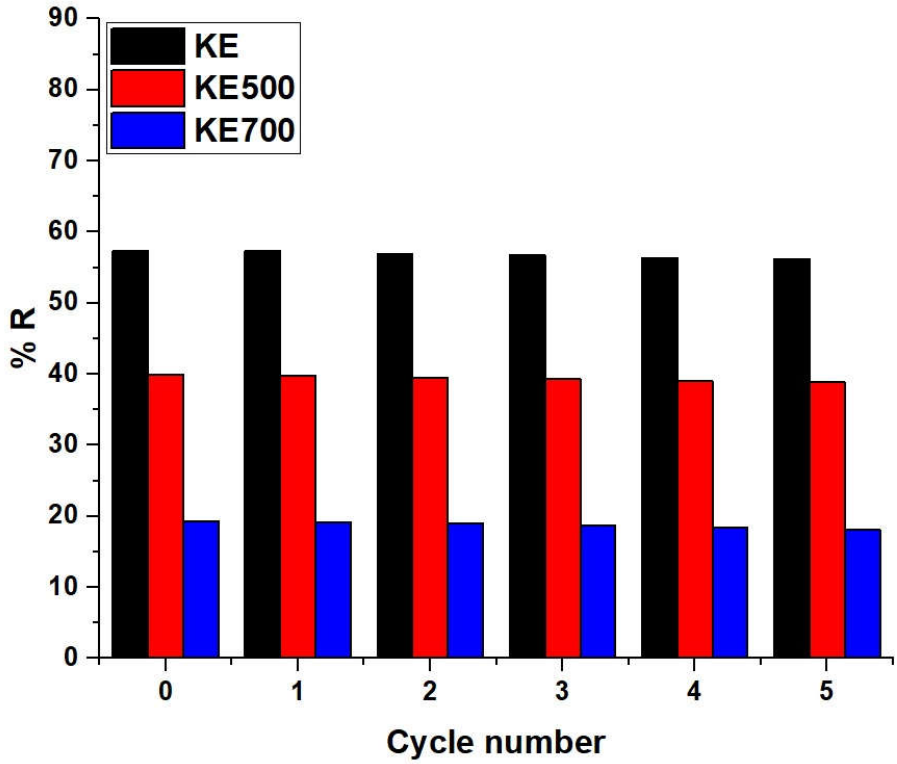

Figure 15. Influence of reusability of the KE, KE500, and KE700 adsorbents on uptake efficacy of BFD dye.

4. Conclusions

Using the Pechini chemical sol–gel procedure, amorphous and crystalline novel adsorbents based on Zr, Mg, Mn, and O were facilely synthesized for the effective elimination of BFD dye from aqueous solutions. Further, the adsorbent, which was synthesized before calcination, was abbreviated as KE. Moreover, the adsorbents, which were synthesized at 500 and 700 °C, were abbreviated as KE500 and KE700, respectively. The KE adsorbent is amorphous, whereas the KE500 and KE700 adsorbents are nanostructured mixtures of ZrO_2, $MgMn_2O_4$, and $Mg(Mg_{0.333}Mg_{1.333})O_4$. The elimination of BFD dye by the KE, KE500, and KE700 products is exothermic, physical, and follows the pseudo-first-order kinetic model and Langmuir equilibrium isotherm. Moreover, the maximum BFD dye uptake capabilities of the KE, KE500, and KE700 adsorbents are 239.81, 174.83, and 93.19 mg/g, respectively.

Author Contributions: Conceptualization, E.A.A.; methodology, E.A.A., M.K. and B.Y.A.; formal analysis, E.A.A. and M.K.; resources, E.A.A. and M.K.; writing—original draft preparation, A.S.A.-W., writing—review and editing, E.A.A. and A.S.A.-W.; funding acquisition, A.S.A.-W. All authors have read and agreed to the published version of the manuscript.

Funding: This research was funded by Princess Nourah bint Abdulrahman University Researchers Supporting Project number (PNURSP2023R35), Princess Nourah bint Abdulrahman University, Riyadh, Saudi Arabia.

Data Availability Statement: Not applicable.

Acknowledgments: The authors are grateful to Princess Nourah bint Abdulrahman University, Riyadh, Saudi Arabia, for funding this work through Researchers Supporting Project number (PNURSP2023R35).

Conflicts of Interest: The authors confirm that there are no conflict of interest for this paper.

References

1. Ahmadian, M.; Jaymand, M. Interpenetrating Polymer Network Hydrogels for Removal of Synthetic Dyes: A Comprehensive Review. *Coord. Chem. Rev.* **2023**, *486*, 215152. [CrossRef]
2. Kausar, A.; Zohra, S.T.; Ijaz, S.; Iqbal, M.; Iqbal, J.; Bibi, I.; Nouren, S.; El Messaoudi, N.; Nazir, A. Cellulose-Based Materials and Their Adsorptive Removal Efficiency for Dyes: A Review. *Int. J. Biol. Macromol.* **2023**, *224*, 1337–1355. [CrossRef] [PubMed]
3. Bilal, M.; Ihsanullah, I.; Hassan Shah, M.U.; Bhaskar Reddy, A.V.; Aminabhavi, T.M. Recent Advances in the Removal of Dyes from Wastewater Using Low-Cost Adsorbents. *J. Environ. Manag.* **2022**, *321*, 115981. [CrossRef]
4. Sankar Sana, S.; Haldhar, R.; Parameswaranpillai, J.; Chavali, M.; Kim, S.C. Silver Nanoparticles-Based Composite for Dye Removal: A Comprehensive Review. *Clean. Mater.* **2022**, *6*, 100161. [CrossRef]
5. Aramesh, N.; Bagheri, A.R.; Bilal, M. Chitosan-Based Hybrid Materials for Adsorptive Removal of Dyes and Underlying Interaction Mechanisms. *Int. J. Biol. Macromol.* **2021**, *183*, 399–422. [CrossRef]
6. Peramune, D.; Manatunga, D.C.; Dassanayake, R.S.; Premalal, V.; Liyanage, R.N.; Gunathilake, C.; Abidi, N. Recent Advances in Biopolymer-Based Advanced Oxidation Processes for Dye Removal Applications: A Review. *Environ. Res.* **2022**, *215*, 114242. [CrossRef] [PubMed]
7. Dadban Shahamat, Y.; Masihpour, M.; Borghei, P.; Hoda Rahmati, S. Removal of Azo Red-60 Dye by Advanced Oxidation Process O_3/UV from Textile Wastewaters Using Box-Behnken Design. *Inorg. Chem. Commun.* **2022**, *143*, 109785. [CrossRef]
8. Wu, S.; Shi, W.; Li, K.; Cai, J.; Xu, C.; Gao, L.; Lu, J.; Ding, F. Chitosan-Based Hollow Nanofiber Membranes with Polyvinylpyrrolidone and Polyvinyl Alcohol for Efficient Removal and Filtration of Organic Dyes and Heavy Metals. *Int. J. Biol. Macromol.* **2023**, *239*, 124264. [CrossRef] [PubMed]
9. Aziz, G.M.; Hussein, S.I.; M-Ridha, M.J.; Mohammed, S.J.; Abed, K.M.; Muhamad, M.H.; Hasan, H.A. Activity of Laccase Enzyme Extracted from Malva Parviflora and Its Potential for Degradation of Reactive Dyes in Aqueous Solution. *Biocatal. Agric. Biotechnol.* **2023**, *50*, 102671. [CrossRef]
10. Ihaddaden, S.; Aberkane, D.; Boukerroui, A.; Robert, D. Removal of Methylene Blue (Basic Dye) by Coagulation-Flocculation with Biomaterials (Bentonite and Opuntia Ficus Indica). *J. Water Process Eng.* **2022**, *49*, 102952. [CrossRef]
11. Abdelrahman, E.A.; Hegazey, R.M.; Ismail, S.H.; El-Feky, H.H.; Khedr, A.M.; Khairy, M.; Ammar, A.M. Facile Synthesis and Characterization of β-Cobalt Hydroxide/Hydrohausmannite/Ramsdellitee/Spertiniite and Tenorite/Cobalt Manganese Oxide/Manganese Oxide as Novel Nanocomposites for Efficient Photocatalytic Degradation of Methylene Blue Dye. *Arab. J. Chem.* **2022**, *15*, 104372. [CrossRef]
12. Khalifa, M.E.; Abdelrahman, E.A.; Hassanien, M.M.; Ibrahim, W.A. Application of Mesoporous Silica Nanoparticles Modified with Dibenzoylmethane as a Novel Composite for Efficient Removal of Cd(II), Hg(II), and Cu(II) Ions from Aqueous Media. *J. Inorg. Organomet. Polym. Mater.* **2020**, *30*, 2182–2196. [CrossRef]
13. Abdelrahman, E.A.; Khalil, M.M.H.; Algethami, F.K.; Khairy, M.; Abou El-Reash, Y.G.; Saad, F.A.; Shah, R.K.; Ammar, A.M. Facile Synthesis of MgO/CuO and MgO/Cu_3MgO_4 Binary Nanocomposites as Promising Adsorbents for the Disposal of Zn(II) Ions. *J. Inorg. Organomet. Polym. Mater.* **2023**. In Press. [CrossRef]
14. Bessy, T.C.; Gatasheh, M.K.; Hatamleh, A.A.; Arokiyaraj, S.; Johnson, J.; Bindhu, M.R. Photocatalytic Degradation of Toxic Dyes and Antimicrobial Activities by Cadmium Doped Magnesium Ferrites Synthesized by Combustion Method. *J. Inorg. Organomet. Polym. Mater.* **2023**. *in press*. [CrossRef]
15. Badawy, A.A.; Ibrahim, S.M.; Essawy, H.A. Enhancing the Textile Dye Removal from Aqueous Solution Using Cobalt Ferrite Nanoparticles Prepared in Presence of Fulvic Acid. *J. Inorg. Organomet. Polym. Mater.* **2020**, *30*, 1798–1813. [CrossRef]
16. Al-Wasidi, A.S.; Saad, F.A.; Munshi, A.M.; Abdelrahman, E.A. Facile Synthesis and Characterization of Magnesium and Manganese Mixed Oxides for the Efficient Removal of Tartrazine Dye from Aqueous Media. *RSC Adv.* **2023**, *13*, 5656–5666. [CrossRef]
17. Mariyam, A.; Shahid, M.; Mantasha, I.; Khan, M.S.; Ahmad, M.S. Tetrazole Based Porous Metal Organic Framework (MOF): Topological Analysis and Dye Adsorption Properties. *J. Inorg. Organomet. Polym. Mater.* **2020**, *30*, 1935–1943. [CrossRef]
18. Ma, T.; Wu, Y.; Liu, N.; Wu, Y. Iron Manganese Oxide Modified Multi-Walled Carbon Nanotube as Efficient Adsorbent for Removal of Organic Dyes: Performance, Kinetics and Mechanism Studies. *J. Inorg. Organomet. Polym. Mater.* **2020**, *30*, 4027–4042. [CrossRef]
19. Danesh, S.M.S.; Faghihian, H.; Shariati, S. Sulfonic Acid Functionalized SBA-3 Silica Mesoporous Magnetite Nanocomposite for Safranin O Dye Removal. *Silicon* **2019**, *11*, 1817–1827. [CrossRef]
20. Abukhadra, M.R.; Mohamed, A.S. Adsorption Removal of Safranin Dye Contaminants from Water Using Various Types of Natural Zeolite. *Silicon* **2019**, *11*, 1635–1647. [CrossRef]
21. Safa, F.; Alinezhad, Y. Ternary Nanocomposite of SiO_2/Fe_3O_4/Multi-Walled Carbon Nanotubes for Efficient Adsorption of Malachite Green: Response Surface Modeling, Equilibrium Isotherms and Kinetics. *Silicon* **2020**, *12*, 1619–1637. [CrossRef]
22. Ba Mohammed, B.; Hsini, A.; Abdellaoui, Y.; Abou Oualid, H.; Laabd, M.; El Ouardi, M.; Ait Addi, A.; Yamni, K.; Tijani, N. Fe-ZSM-5 Zeolite for Efficient Removal of Basic Fuchsin Dye from Aqueous Solutions: Synthesis, Characterization and Adsorption Process Optimization Using BBD-RSM Modeling. *J. Environ. Chem. Eng.* **2020**, *8*, 104419. [CrossRef]
23. Khan, T.A.; Khan, E.A. Shahjahan Removal of Basic Dyes from Aqueous Solution by Adsorption onto Binary Iron-Manganese Oxide Coated Kaolinite: Non-Linear Isotherm and Kinetics Modeling. *Appl. Clay Sci.* **2015**, *107*, 70–77. [CrossRef]

24. Ai, L.; Jiang, J. Fast Removal of Organic Dyes from Aqueous Solutions by AC/Ferrospinel Composite. *Desalination* **2010**, *262*, 134–140. [CrossRef]
25. Hinojosa-Reyes, M.; Camposeco-Solis, R.; Ruiz, F. $H_2Ti_3O_7$ Titanate Nanotubes for Highly Effective Adsorption of Basic Fuchsin Dye for Water Purification. *Microporous Mesoporous Mater.* **2019**, *276*, 183–191. [CrossRef]
26. Apostol, I.; Anghel, N.; Doroftei, F.; Bele, A.; Spiridon, I. Xanthan or Esterified Xanthan/Cobalt Ferrite-Lignin Hybrid Materials for Methyl Blue and Basic Fuchsine Dyes Removal: Equilibrium, Kinetic and Thermodynamic Studies. *Mater. Today Chem.* **2023**, *27*, 101299. [CrossRef]
27. Bichave, M.S.; Kature, A.Y.; Koranne, S.V.; Shinde, R.S.; Gongle, A.S.; Choudhari, V.P.; Topare, N.S.; Raut-Jadhav, S.; Bokil, S.A. Nano-Metal Oxides-Activated Carbons for Dyes Removal: A Review. *Mater. Today Proc.* **2022**, *77*, 19–30. [CrossRef]
28. Al-Ghouti, M.A.; Khan, M.; Malik, A.; Khraisheh, M.; Hijazi, D.; Mohamed, S.; Alsorour, S.; Eltayeb, R.; Al Mahmoud, F.; Alahmad, J. Development of Novel Nano-γ-Al_2O_3 Adsorbent from Waste Aluminum Foil for the Removal of Boron and Bromide from Aqueous Solution. *J. Water Process Eng.* **2022**, *50*, 103312. [CrossRef]
29. Alizadeh, Z.; Rezaee, A. Tetracycline Removal Using Microbial Cellulose@nano-Fe_3O_4 by Adsorption and Heterogeneous Fenton-like Processes. *J. Mol. Liq.* **2022**, *366*, 120199. [CrossRef]
30. Xiong, C.; Wang, W.; Tan, F.; Luo, F.; Chen, J.; Qiao, X. Investigation on the Efficiency and Mechanism of Cd(II) and Pb(II) Removal from Aqueous Solutions Using MgO Nanoparticles. *J. Hazard. Mater.* **2015**, *299*, 664–674. [CrossRef] [PubMed]
31. Mahdi, M.A.; Jasim, L.S.; Ranjeh, M.; Masjedi-Arani, M.; Salavati-Niasari, M. Improved Pechini Sol-Gel Fabrication of $Li_2B_4O_7$/NiO/$Ni_3(BO_3)_2$ Nanocomposites to Advanced Photocatalytic Performance. *Arab. J. Chem.* **2022**, *15*, 103768. [CrossRef]
32. Shojaei, B.; Miri, R.; Bazyari, A.; Thompson, L.T. Asphaltene Adsorption on MgO, CaO, SiO_2, and Al_2O_3 Nanoparticles Synthesized via the Pechini-Type Sol−Gel Method. *Fuel* **2022**, *321*, 124136. [CrossRef]
33. Ranjeh, M.; Beshkar, F.; Amiri, O.; Salavati-Niasari, M.; Moayedi, H. Pechini Sol-Gel Synthesis of Cu_2O/Li_3BO_3 and CuO/Li_3BO_3 Nanocomposites for Visible Light-Driven Photocatalytic Degradation of Dye Pollutant. *J. Alloys Compd.* **2020**, *815*, 152451. [CrossRef]
34. Mirzaei, A.; Janghorban, K.; Hashemi, B.; Bonyani, M.; Leonardi, S.G.; Neri, G. Highly Stable and Selective Ethanol Sensor Based on α-Fe_2O_3 Nanoparticles Prepared by Pechini Sol-Gel Method. *Ceram. Int.* **2016**, *42*, 6136–6144. [CrossRef]
35. Alhaji, A.; Razavi, R.S.; Ghasemi, A.; Loghman-Estarki, M.R. Modification of Pechini Sol–Gel Process for the Synthesis of MgO-Y_2O_3 Composite Nanopowder Using Sucrose-Mediated Technique. *Ceram. Int.* **2017**, *43*, 2541–2548. [CrossRef]
36. Krishna Kumar, A.S.; Warchol, J.; Matusik, J.; Tseng, W.L.; Rajesh, N.; Bajda, T. Heavy Metal and Organic Dye Removal via a Hybrid Porous Hexagonal Boron Nitride-Based Magnetic Aerogel. *Npj Clean Water* **2022**, *5*, 24. [CrossRef]
37. Kalidhasan, S.; Santhana Krishna Kumar, A.; Rajesh, V.; Rajesh, N. Enhanced Adsorption of Hexavalent Chromium Arising out of an Admirable Interaction between a Synthetic Polymer and an Ionic Liquid. *Chem. Eng. J.* **2013**, *222*, 454–463. [CrossRef]
38. Radha, F.H.S.; Shwan, D.M.S.; Kaufhold, S. Adsorption Study and Removal of Basic Fuchsin Dye from Medical Laboratory Wastewater Using Local Natural Clay. *Adsorpt. Sci. Technol.* **2023**, *2023*, 9398167. [CrossRef]
39. Labiod, K.; Hazourli, S.; Bendaia, M.; Tlili, M.; Aitbara, A.; Graine, R.; Meradi, H. Removal of Azo Dye Carmoisine by Adsorption Process on Diatomite. *Adsorpt. Sci. Technol.* **2022**, *2022*, 1–17. [CrossRef]
40. Abdullah, E.A.; Abdullah, A.H.; Zainal, Z.; Ban, T.K.; Material, A. Bismuth Basic Nitrate as a Novel Adsorbent for Azo Dye Removal. *J. Chem.* **2012**, *9*, 1885–1896. [CrossRef]